ELSEVIER

Cement & Concrete Composites 23 (2001) 279–287

Cement & Concrete Composites

www.elsevier.com/locate/cemconcomp

A model for computation of leakage through damaged concrete structures

H. Boussa [a], C. Tognazzi-Lawrence [a,b], C. La Borderie [a,*]

[a] LaSAGeC, ISA BTP, Allée du Parc Montaury, 64 600 Anglet, France
[b] LMDC, INSA-UPS GC, Rangueil, 31077 Toulouse cedex 04, France

Abstract

Predictive computation of fluid flows through concrete structures subjected to mechanical and/or thermal loading requires detailed description of cracks. A series of experiments were performed to obtain statistical data on the crack profile. For that purpose, concrete specimens were cracked using bending tests. Three concrete mixtures with the same aggregate were used to illustrate the difference between normal and high-performance concrete. Three-point and four-point bending tests were conducted so that the role of the stress gradient on the roughness was assessed. The obtained cracks were scanned and their geometry was digitized and statistically studied. A probabilistic crack-generation model based on previous results allowed to generate crack patterns at the microscale level according to the given field of damage at the macroscale level. The obtained computed crack pattern was used for flow computation. It was shown that the probabilistic model produced statistically representative results for the flow computation. The influence of parameters like crack opening, pressure, and roughness were then evaluated.

Keywords: Crack geometry; Picture analysis; Damage; Fluid flow; Model; Computation

1. Introduction

In civil engineering, many structures act as tight barriers that can impede, or, at least slow down, the mass transport process between two media. One can mention, for example: containers and structures for waste storage, pipes, nuclear containment, and dams.

Today, it is possible to obtain some satisfactory predictions for the mechanical behavior of such structures subjected to mechanical and/or thermal loading, from a global point of view (displacement at specific points, actions of support, etc...) and equally from a local point of view (state of cracking – cracks position and openings, stress, etc...). However, when predictions must relate to a leakage rate, it is necessary to extrapolate the mechanical results and then to use a specific model of fluid flow. Because the internal scales linked to damage propagation and to fluid flow are completely different, it is not possible to use directly the mechanical result for performing the fluid flow computation. The geometrical description of a crack obtained from the first computation must be enhanced.

In the presence of macrocracks, most of the flow leaks through these cracks. Models currently available in the literature for flow through macrocracks are based on a Poiseuille's law corrected by a coefficient of tortuosity, whose value is difficult to determine. If these kinds of models are nowadays correctly established in the case of microcracks or low differential pressure, in the case of wide openings and high differential pressure, they are not able to predict the flow rate with a correct accuracy.

Our process consists of modeling the flow with the same level of sophistication as in mechanics, i.e., to directly discretize the Navier–Stokes equations [1].

The major problem lies in the transition from solid mechanics to fluid mechanics. Scales of modeling are completely different and mechanical results for cracking obtained from non-linear finite element computations cannot be used directly for the flow calculation. When performing non-linear computation of concrete structure, the heterogeneity of the material and strain softening leads to strain localization and must be modeled with a regularization method. Localization and regularization methods for strain-softening models are the

* Corresponding author. Fax: +33-5-59-57-70-02.
E-mail address: christian.laborderie@univ-pau.fr (C. La Borderie).

0958-9465/01/$ - see front matter
PII: S0958-9465(00)00063-9

subject of a lot of papers. Discrete approaches [2,3] or continuum modeling [4–6] illustrates an internal length scale which is about five times the size of the coarsest aggregate. This is the correct scale for the non-linear mechanical computations using damage mechanics [7–9, among others] or smeared crack approach [10]. This scale is called the macroscale in what follows. It is then possible to consider the material as homogeneous and continuous.

The correct scale for the flow computation is called the microscale. The characteristic dimension for a correct description of the tortuosity and the roughness of the crack is about one-tenth of the crack opening, i.e. 0.01 mm at the most. Smaller scales are present in the crack geometry, which could be considered a fractal property [11], but they would not affect transfer, so they are not essential for the flow computation.

2. Experimental procedure to determine the crack geometry

To construct a realistic crack profile for the leakage computation, it was proposed to compose it of straight line segments. Each segment represented the part of the crack growing through or avoiding a granulate. A series of bending tests to obtain a cracked specimen were performed to study crack geometry. Statistical data of crack geometry experiments were analyzed in terms of deviation angles and segment lengths (Fig. 1).

2.1. Mechanical test

Three concrete mixtures (see Table 1 for composition) with the same aggregate ($D_{max} = 16$ mm), and approximately the same paste content were tested to investigate the difference between normal and high-performance concrete. $100 \times 100 \times 500$ mm^3 plain concrete prisms were cured for at least 28 days at 100% R. H. and 20°C until the day of testing.

In addition, it was interesting to know if the stress gradient at the crack tip influences the geometry of the crack.

Three-point and four-point bending tests were performed for each mixture to underline the role of the stress gradient and the paste characteristics on the roughness of the crack (see Table 2).

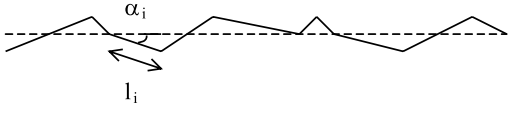

Fig. 1. Example of a crack geometry constituted from linear segments with various lengths and orientation angles.

Table 1
Compositions and principal characteristics of tested concrete

	Ordinary concrete C30	HPC C60	HPC C80
Cement (kg/m^3)	350	400	450
Aggregate with	1900	1900	1860
Sand (kg/m^3)[a]	760	741	725
Grit and gravel (kg/m^3)	1140	1159	1135
Total amount of water (l/m^3)	208.7	176	148
Plasticizer resin GT (%)	–	1	4
W/C	0.59	0.44	0.33
Vol. of paste[b] (l/m^3)	320	300	290
Vol. of matrix[c] (l/m^3)	365	330	330
Density	2.44	2.49	2.54
Slump (mm)	90	>250	200
fc_{28} (MPa)	33.9	59.3	80.0

[a] Sand is a mix of four sands. It varies little from one concrete to another and contains between 10% and 16.5% of fines ($d < 100$ μm).
[b] Paste = cement + water + additive.
[c] Matrix = cement + water + additive + fines from sand ($d < 100$ μm).

Table 2
Number of performed tests

	C30	C60	C80
3-point bending	4	3	3
4-point bending	1	1	0

The mechanical tests were performed until the breaking of the specimen, and only the final crack was observed. These experiments were performed under load control, so that it is difficult to give the value of the crack-propagation celerity. This parameter can affect the roughness of the crack and must, on evidence, be evaluated on further experiments.

The fracture surface of each part of the broken specimen was molded with cement paste containing a red pigment (white cement and 1.5% by mass of Ferro oxide). This red pigment offered the best contrast between the molding part and matrix, and between the molding part and aggregate.

The central part of the specimens were cut in four slices 15 mm thick, so that eight fracture profiles were observed for each half of the specimen among its 100 mm width. As the required geometry resolution for this study was only 40 μm and the surface irregularities produced by the saw were much smaller, no other preparation (grinding or polishing) of the concrete sections was necessary.

2.2. Data acquisition and picture binarization

The color images were scanned with an optical resolution of 600 dpi. The size of each pixel was 40 μm. This simple method for image acquisition was proved to be a

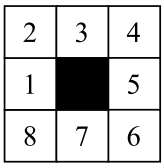

Fig. 2. Freeman notation.

good compromise considering the optical materials available at the laboratory, the computing capacity for image analysis, and the required resolution. Each sample being 100 m high, the whole fracture could be stored in only one ($2500 \times n$) pixels image (with n variable in function of profile).

This digitized color image was first binarized with the software VISILOG5 and then the binarized image was analyzed to extract the fracture profile with an image analysis program previously developed at LMDC (and used for example in [12]), and based on mathematical morphology [13,14].

The color image was automatically filtered in an HLS image (hue, luminescence, saturation), then transformed in three images H, L and S. An automatic thresholding on canal S gave a binary image (in some cases, big errors of thresholding were noted, so a half-automatic thresholding was made on the HLS image giving an interest zone in the red cement paste). A first operation of holes filling on the two parts of the image (the concrete in black and the red cement paste in white) was then performed before the new binary image was analyzed to extract the fracture profile.

The binary image was in square grid with eight connexity. Extraction involved a series of erosion, building, closure and thinning operations until the fracture profile appeared as a line one pixel wide. The line obtained was then described as a series of pixels and was coded using the Freeman notation: the Freeman code gives the relative position of a pixel towards its predecessor with a number from 1 to 8, as in Fig. 2. As a result, the whole profile was stored as a list of numbers from 1 to 8.

2.3. Vectorization

As the required description of the fracture profile was not in terms of unitary segment and angle, the form of the line was analyzed further with an iterative method to find the best series of straight segments fitting the line.

As an example, let us consider the two segments shown in Fig. 3(a), of which the digitized picture is displayed in Fig. 3(b). The corresponding freeman series is: 7667667667667667667667667667667667688887888888888788888888878.

In order to use the original picture 3(a), we cannot consider that there is a series of 60 unit segments but of 2 segments.

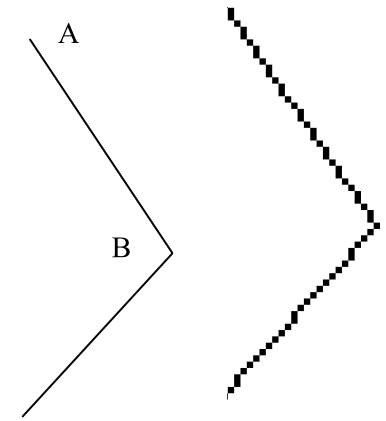

Fig. 3. Example of vectorization.

Knowing a characteristic point A, one must find the next point B. The criterion used was that the distance between any pixel flanked by A and B and the line AB had to be smaller than a given value $\tilde{\delta}$.

Using the first pixel as a characteristic point, this process is repeated until the end of the line.

For this analysis, $\tilde{\delta}^2 = 1.5h^2$ was used, where h was the size of the pixel ($h = 40$ μm).

Fig. 4 gives an example of image analysis operations.

3. Statistical analysis of the crack geometry

The 73 crack profiles obtained from the experiments were statistically analyzed to build a probabilistic generation model for crack geometry. These results were used for studying the role of the stress gradient and the concrete composition on crack geometry, and therefore on the crack generation model.

The crack geometry was described by means of a series of linear segments as shown in Fig. 1. The length and the angle deviation of these segments were the two statistical variables studied in what follows.

Firstly, frequencies of these variables were computed for each profile, and then histogram curves were plotted and studied.

3.1. Angle distribution

Due to the bell shape of the angle distribution curve (Fig. 5), one can expect a normal distribution function. A continuous normal distribution is characterized by the values of the skewness $\gamma_1 = 3$ and discrepancy $\gamma_2 = 0$, where

$$\gamma_1 = \frac{\mu_3}{\sigma^3},$$

where $\mu_3 = E[(X - m)^3]$, and m is the average.

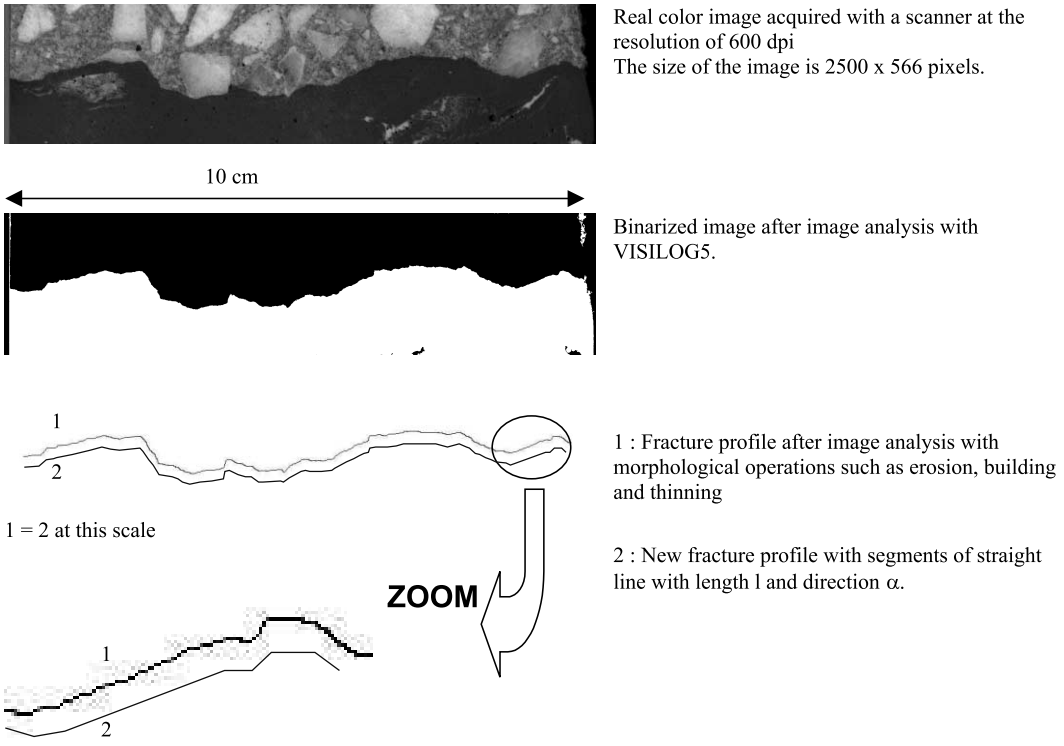

Fig. 4. Image analysis operations.

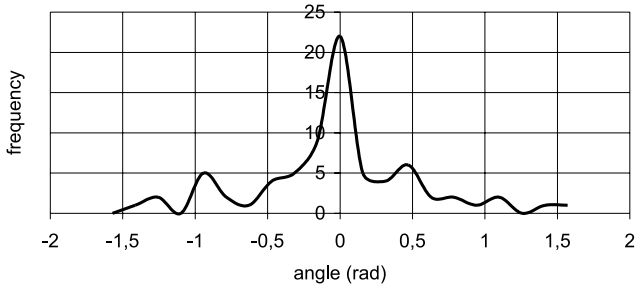

Fig. 5. Typical angle distribution for a C60.

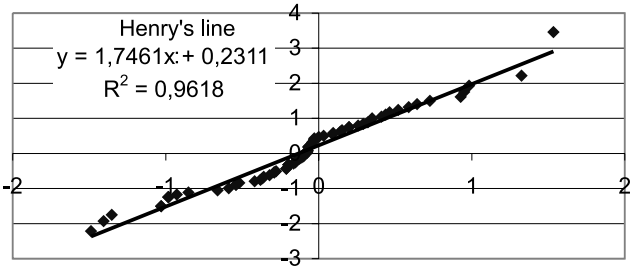

Fig. 6. Typical Henry's line for a C60 angle distribution.

$$\gamma_2 = \frac{\mu_4}{\sigma^4},$$

where $\mu_4 = E[(X - m)^4]$, and σ is the SD.

For a discrete distribution, the statistical tables [15] give the critical values of these coefficients for various sample sizes (between 60 and 100 samples depending on the distribution). The confident interval, larger than 98% for most distributions proved that a normal law was well suited.

The nature of these distributions was also tested by means of the Henry's line method. When observations x_i come from a normal law of average m and SD σ, the values $u_i = (x_i - m)/\sigma$ constitute a distribution of a non-dimensional normal-centered variable (NDNCV).

For each cumulated frequency F_i of x_i, we have associated $u_i^* = \phi^{-1}(F_i)$ where ϕ is the distribution function of the NDNCV. For a normal distribution, a linear relationship between u_i^* and x_i should be obtained and the regression factor R gives the availability of such distribution (Fig. 6).

The mean regression factor R^2 for Henry's lines for all specimens was 0.94 and confirmed the normality of the angle distribution.

The mean value of the angle distribution is specific for a global rotation of the crack, so only the SD was studied (Fig. 7).

3.2. Length distribution

The shape of the histogram curves of the lengths' distributions were strongly asymmetric (Fig. 8) and suggested the use of a log-normal law.

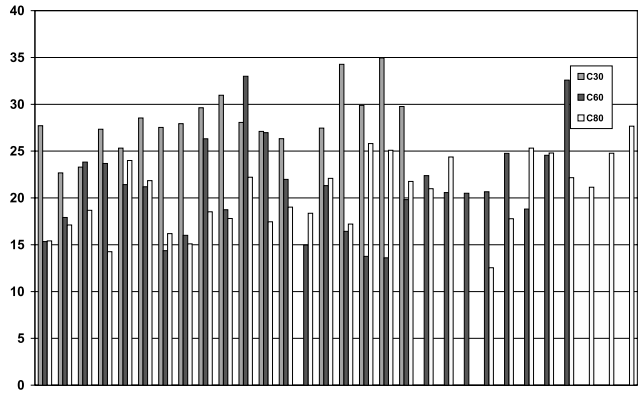

Fig. 7. SD of the angle.

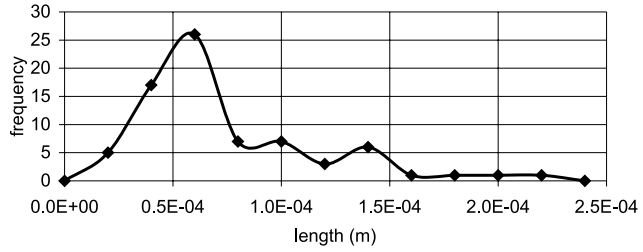

Fig. 8. Typical length distribution for a C60.

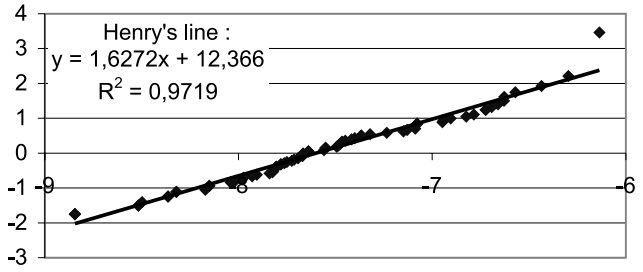

Fig. 9. Typical Henry's line for a C60 length distribution.

The variable change $X = \ln L$ was carried out, where L was the segment's length. The above-described method was used to establish the normality of X, and consequently the log-normality of the length distribution (Fig. 9).

The results are summarized in Table 3. According to Table 2, 12 specimens were tested and 73 crack profiles analyzed.

3.3. Influence of the concrete mixture

Since the three concrete mixtures use the same aggregate, one could expect that the number of transgranular crack segments would increase with the matrix strength. This would imply a decrease of the angle SD.

This fact was confirmed when comparing C60 with C30 and C80 with C30. With the concrete mixtures used, cracks were already transgranular with a C60 and then the angle deviation remained nearly constant between C60 and C80.

The effect of the concrete mixture on the segment length was not obvious.

3.4. Influence of the stress gradient

Based on structural considerations, the tortuosity of the crack, and consequently the SD of the angle, should decrease a priori with the stress gradient. This effect is not obvious on the shown results in Table 3, especially for the C30.

There is no visible effect of the stress gradient on the length segment.

In conclusion, the role of the stress gradient is not emphasized in the present results. It seems reasonable to neglect its effects on the roughness of the crack. Otherwise, the strength of the matrix affects the SD of the angle until cracks are transgranular. More experiments must be done on additional concrete mixtures in order to refine these results.

4. Numerical crack pattern

As we intended to perform a complete computation of any structure, from the virgin structure subjected to

Table 3
Statistical data for cracks

Concrete mixture	Number of bending points	Number of analysed cracks	Angle (degrees)				Length (mm)			
			Mean		SD		Mean		SD	
C30	3	11	−2.2	−4.6	29.4	28.3	0.58	0.57	0.31	0.30
	4	5	−10.9		25.3		0.54		0.28	
C60	3	19	−4.2	−3.9	20.0	21.0	0.67	0.68	0.36	0.37
	4	8	−3.3		23.1		0.71		0.40	
C80	3	30	−6.3	−6.3	19.6	19.6	0.64	0.64	0.39	0.39
	4	–	–		–		–		–	

mechanical and thermal loading to the flow of a gas or a liquid through the cracks, the number, the position and the opening of cracks were predicted at the structural level. Then, the fluid flow was simulated at a microscale level.

The structural level was modeled by way of a finite element calculation using non-linear continuum mechanics (damage, smeared crack, microplanes,...etc). It was assumed at this level that the disorder of the material was correctly represented by the material behavior model and the regularization method. The results obtained were fields of internal variables that must be enriched to obtain a crack geometry which was representative of the fluid flow. Statistical results presented previously were used to bring a probabilistic enrichment.

Thus, the final computed crack profile used for the fluid computation was the result of two embedded models:

- the mechanical model that gave the mean line and the opening of the crack;
- the probabilistic model based on the previous statistical study that gave a more realistic profile of the crack lips.

4.1. Enrichment method designed for fluid flow analysis

Different physical scales must be taken into account for the mechanical computation of a structure and for the leak rate computation into a crack pattern. For the computed crack pattern to be representative of the real pattern towards the flow, it is necessary to enrich the mechanical results. The deviations of a real crack pattern compared to the theoretical pattern obtained with the hypothesis of a homogeneous material are due to the heterogeneity of the material. Even with the significant progress of computers, structural computations that include the modeling of heterogeneity still cannot be used effectively. Nevertheless, heterogeneity can be taken into account through a post-treatment of a homogeneous computation.

Results of the mechanical computation give continuous fields of a variable that represents the damage of material. A first step, i.e. transition from continuum to the discrete description, must be achieved in order to get some average lines for cracks (those called theoretical cracks) and the crack openings (Fig. 10).

Then, a more realistic crack pattern can be obtained as a deviation of the theoretical one. Furthermore, as cracking is a discontinuity into an originally continuous medium, the two crack lips are supposed to have the same profile (disregarding the crack opening).

The crack profile is built with segments of a straight line. The length of each segment, and the angle between each segment and the theoretical pattern, are distributed according to the previous study and are randomly and independently drawn. For mechanical reasons, the angle cannot be greater than 90°.

Fig. 11 shows a sample obtained from the theoretical crack pattern (the crack opening is scaled by 100 in this figure).

4.2. From the continuum to the discrete

The use of a regularization method is a necessary way to obtain predictive results of computation until the structure breaks. Whatever the method used, an internal length appears in the computation. This internal length makes it possible to pass from the continuum to a discretized material.

The method used was derived from Hillerborg's work and it used an energy equivalence [2,3]. This method is efficient when the crack is localized across a band of elements but is not suitable to predict the crack pattern for distributed cracks.

The inelastic strains can be calculated as follows:

$$\varepsilon_{ij}^{\text{in}} = \varepsilon_{ij} - S_{ijkl}^{\text{e}}\,\sigma_{kl},$$

where S_{ijkl}^{e} is the elastic flexibility matrix of the material.

The total crack opening along a direction given by the unit vector n can be calculated as follows:

$$\delta_n = \int_{\text{element}} \varepsilon_{ij}^{\text{in}}\, n_i\, n_j \,\mathrm{d}x_n,$$

with x_n the abscissa along the vector n.

The position of the crack in the element can be considered as the pressure center. This supposition gives a continuous crack pattern through the elements.

Fig. 10. Crack obtained from a structural computation using continuum damage mechanics.

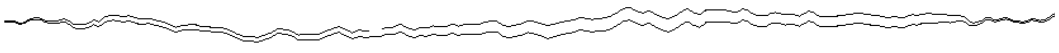

Fig. 11. Realistic crack.

Given the moment M_n,

$$M_n = \int_{\text{element}} x_n \varepsilon_{ij}^{\text{in}} n_i n_j \, \mathrm{d}x_n,$$

the position X_c of the crack into the considered element is given by,

$$X_c = \frac{M_n}{\delta_n}.$$

The total crack opening splits into macrocracks which contribute to the flow design, and microcracks that constitute the fracture process zone [11].

As a first approximation, according to the study of Mivelaz [16], half of the inelastic strains are shared into microcracks and the other half into macrocracks.

The obtained crack profile as shown on Fig. 11 was used for the mesh generation of the fluid flow computation and for the leakage.

5. Fluid flow analysis

As a first result, only bidimensional results and constant crack openings are discussed here, even if tridimensional computations are available [1]. The goal of the present studies is only to determine if the model is statistically stable, and to observe the physical phenomena that governs the flow. We can notice that in case of non-constant opening, the variation of opening is generally slow enough to consider it as piecewise constant.

Assuming an incompressible, steady, constant fluid and two-dimensional flow, the governing differential equations for the present flow are the conservation of mass and the Navier–Stokes equations

$$\frac{\partial U}{\partial X} + \frac{\partial V}{\partial Y} = 0,$$

$$U\frac{\partial U}{\partial X} + V\frac{\partial U}{\partial Y} = -\frac{1}{\rho}\frac{\partial P^*}{\partial X} + v\left(\frac{\partial^2 U}{\partial X^2} + \frac{\partial^2 U}{\partial Y^2}\right),$$

$$U\frac{\partial V}{\partial X} + V\frac{\partial V}{\partial Y} = -\frac{1}{\rho}\frac{\partial P^*}{\partial Y} + v\left(\frac{\partial^2 V}{\partial X^2} + \frac{\partial^2 V}{\partial Y^2}\right),$$

where ρ is the density of the fluid, v the kinematic viscosity, P^* the dynamic pressure, and U and V are the velocity components.

The computation of the Navier–Stokes equations was accomplished by Finite Element method.

The crack in concrete was meshed with 8-node isoparametric quadrilateral elements, and the crack lips were generated using the previously presented probabilistic model.

To capture correctly the higher velocity gradients in the crack, a high mesh density was used across the width (20 elements). Since the velocity gradient was higher near the boundaries, the mesh was more refined around the crack lips than in the middle of the crack cross-section.

The length of the crack in our example was 50–200 times greater than the opening, it was necessary to use an element whose size was lower than 0.1 mm along the crack to avoid flat elements. Fig. 12 shows a typical distribution of grid points for a small part of a crack with a length of 5 mm.

The complete Finite Element model encompassed 38 907 nodes and 37 696 elements.

A zero value for the normal and tangential velocity was imposed on the crack lips and uniform values of pressure were imposed on the inlet and outlet sections.

As a first example, the computation of the leak rate was performed for three crack profiles obtained by the crack probabilistic generation model for the same parameters.

If the model is representative of crack geometry regarding the fluid flow, we should obtain similar results for the three computations.

The three crack patterns are presented in Fig. 13.

The following parameters were taken for the fluid, here, air, (used for the leak tests of containment walls of nuclear reactors), as an example:

density of the fluid (kg/m^3)	1.23
kinematic viscosity (m^2/s)	1.18×10^{-5}
pressure gradient (Pa/m)	2×10^2, 2×10^4, 5×10^4, 2×10^5, 5×10^5, 8×10^5

The flow rates obtained for the three random samples shown in Fig. 13, with a crack opening of 0.1 mm, were compared for the six different values of the pressure gradient (Fig. 14). The variations in the results obtained were less than 10%, so the model could be considered as statistically valid and representative of crack geometry concerning fluid flow.

Then, the following parameters were used for the crack geometry.

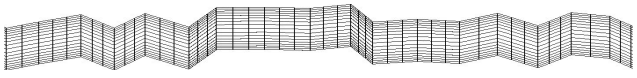

Fig. 12. Crack mesh.

Fig. 13. Generation of three random crack patterns (crack length: 50 mm; SD of the angle: 30°; mean of the length segments: 0.5 mm; SD of the length segments: 0.25).

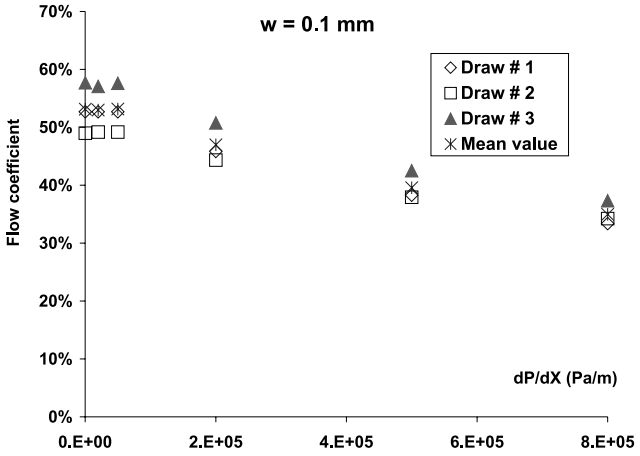

Fig. 14. Flow rates for the three random cracks shown in Fig. 13.

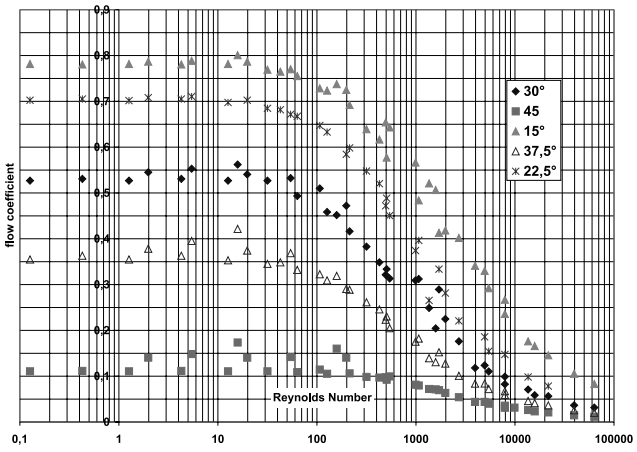

Fig. 16. Influence of the SD of the angle on the flow coefficient for different Reynolds numbers.

crack length	50 (mm)
constant crack opening	0.05–1 (mm)
SD of the angle	15°, 22.5°, 30°, 37.5°, 45°
mean of the segment length	0.05–0.75 (mm)
SD of the segment length	0.5 × mean value

In contrast to experiments, local flow parameters were available and provided a better understanding of the physical parameters that govern the flow. For example, we could compare the velocity fields obtained for different pressure gradients for the same crack.

For a low value of the pressure gradient, and then for a low value of the Reynolds number, the velocity field was typical of a laminar steady state flow and showed a parabolic distribution in the crack cross-section (Fig. 15(a)), the flow was not modified by the roughness of the crack. At a higher pressure gradient (Fig. 15(b)), some areas of recirculating secondary flows appeared even if the main flow stayed laminar, and the role of the crack profile became relevant.

The role of different parameters of the model have been evaluated, and as an example, Fig. 16 shows the influence of the SD of the angle on the flow coefficient for different values of the Reynolds number.

6. Conclusion

A probabilistic model based on experiments enables to switch from the macroscale to the microscale level.

- On one hand, a mechanical model gives the mean line and the opening of cracks.
- On the other hand, the crack probabilistic generation model gives a more realistic profile of these cracks: cracks are constituted from linear segments. Their lengths and orientation angles are statistically distributed according to experimental results and randomly drawn.

The probabilistic model is representative of crack geometry as regards fluid flow.

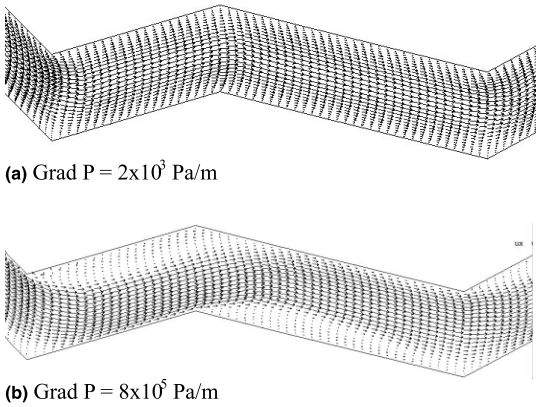

(a) Grad P = $2x10^3$ Pa/m

(b) Grad P = $8x10^5$ Pa/m

Standard deviation of the angle : 30 °
Mean length of segment : 0.5 mm
Standard deviation of the length : 0.25 mm
Constant crack opening : 0.25 mm

Fig. 15. Flow configurations for two different pressure gradients.

The method used for leakage computation through cracks shows that the flow is of a very complex structure even at low Reynolds numbers and it is demonstrated that the roughness of the crack lips is a very important parameter which cannot be easily modeled by the way of a simple scalar parameter.

Thus, the developed method is useful for a better understanding of the flow through cracks, for a direct use on leakage computation or for building simplified models.

As a first direct application, the model was used for the predictive computation of the leakage of a large-scale model of a reinforced and prestressed concrete wall containment subjected to a thermo-mechanical loading [17]. The macrocrack position and openings were predicted with the use of a thermomechanical non-linear computation, then the cracks' geometry was generated with the previously presented model and fluid flow computations were performed. Our results agree with the experiments and give better predictions compared to the results of other competitors of the corresponding benchmark [18].

From a more general point of view, the principle of two embedded models can be employed for coupling between cracking and phenomena that have a lower internal length scale like diffusion, chemical reaction etc., ...

Acknowledgements

The Electrité de France (EDF/Septen) and the European Community are gratefully acknowledged for the support of this Study. E. Ringot (LMDC, Toulouse, France) is acknowledged for the experiments and the image analysis.

References

[1] Boussa H. Structures en béton soumises à des sollicitations thermomécaniques sévères: prévision des dommages et des évolutions de perméabilités. Thesis, ENS Cachan, France: January 2000.

[2] Hillerborg A, Modeer M, Petersson PG. Analysis of crack formation and crack growth in means by fracture mechanics and finite elements. Cem Concr Res 1976;6:773–86.

[3] Hillerborg A. In: Wittmann FH, editor. Analysis of one single crack. Fracture mechanics of concrete. Amsterdam: Elsevier BV; 1983. p. 223–49.

[4] Pijaudier-Cabot G, Bazant ZP. Non local damage theory. ASCE J Eng Mech 1987;133:1512–33.

[5] De Borst R. Simulation of strain localization: a reappraisal of the Cosserat continuum. Eng Comput 1991;83:3317–32.

[6] De Borst R, Mülhaus H-B. Gradient dependent plasticity: formulation and algorithmic aspects. Int J Num Meth Eng 1992;35:521–39.

[7] Mazars J, Pijaudier-Cabot G. Continuum damage theory – application to concrete. ASCE J Eng Mech 1989;155:345–65.

[8] La Borderie C, Mazars J, Pijaudier-Cabot G. In: Gerstle W, Bazant ZP, editors. Damage mechanics model for RC structures under cyclic loading. ACISP 134; 1994. p. 147–72.

[9] Fichant S, Pijaudier-Cabot G, La Borderie C. Continuum damage modelling: approximation of the crack induced anisotropy. Mech Res Commun Basic and Implied March-April 1997;24(2).

[10] Rots JG. Computational modeling of concrete fracture. Dissertation, Delft University of Technology; 1988.

[11] Bazant ZP. ACI committee on Fracture Mechanics, Fracture mechanics of concrete: concepts, models and determination of material properties. Detroit: ACI Special publication; 1991.

[12] Al Hassani Y, Bascoul A, Ringot E. Reconnaissance automatique de la microfissuration des bétons, Compte -rendu de la 1^{ére} réunion annuelle GEO. Aussois, France; 21–25 November 94.

[13] Beucher S. Segmentation d'Images et Morphologie Mathématique. Ph.D. thesis, Ecole des Mines, Paris; 1990.

[14] Coster M, Chermant J-L. Précis d'analyse d'image, second ed.. Paris: Presses du CNRS; 1989.

[15] Saporta G. Probabilités, Analyse des données et Statistique. éditions TECHNIP;1990.

[16] Mivelaz P. Etancheité des structures en béton armé- fuites au travers d'un élément fissuré. Thesis, EPF Lausanne no. 1539; 1996.

[17] Granger L, Al. A mock up near Civaux nuclear plant for containment evaluation under severe accident, the CESA project. In: Proceedings of SMIRT. Lyon, France; December 1997.

[18] Valfort JL. Containment evaluation under severe accident – analysis of the results – Leak rate analysis. Framework program on nuclear fission safety. European Commission contract F14S-CT96-0026 report; April 2000.